Characterization of Fe−MCM-41 Molecular Sieves with Incorporated Carotenoids by Multifrequency Electron Paramagnetic Resonance

Tatyana A. Konovalova, Yunlong Gao, and Lowell D. Kispert*

Department of Chemistry, Box 870336, University of Alabama, Tuscaloosa, Alabama 35487

Johan van Tol and Louis-Claude Brunel

Center for Interdisciplinary Magnetic Resonance, National High Magnetic Field Laboratory, Florida State University, Tallahassee, Florida 32310

Received: July 8, 2002; In Final Form: November 25, 2002

Multifrequency electron paramagnetic resonance (EPR) spectroscopy was applied to study Fe(III)−MCM-41 mesoporous molecular sieves with incorporated carotenoids. It was demonstrated that high-frequency/high-field EPR is a promising technique to increase spectral resolution for proper assignment of different Fe^{3+} sites, which cannot be resolved by the X-band experiments. The broad unresolved at 9 GHz EPR line in the $g = 2$ region is due to overlapping signals from Fe^{3+} sites with different zero field parameters. The peak with $g = 2.45$ is tentatively assigned to aggregated Fe^{3+}. The signal with $g = 2.07$ can be attributed to Fe^{3+} coordinated to oxygen atoms on the surface of the pore. A narrow line with $g_x = g_y = 2.003$, $g_z = 1.99$, and $E/D = 0.3$ was attributed to a single Fe^{3+} site. The X-band and 94 GHz EPR measurements indicated that extraframework iron species at the surface of the mesopores are mostly responsible for carotenoid oxidation in molecular sieves. ENDOR measurements revealed the orientation of 7′-apo-7′,7′-dicyano-β-carotene and canthaxanthin within Fe−MCM-41.

Introduction

Incorporation of transition metal ions into the framework of molecular sieves has received considerable attention over the past few years due to the new catalytic properties of the modified materials. Although unique catalytic activities of iron-containing zeolites have been widely discussed,[1−3] catalytic properties of Fe-modified MCM-41 molecular sieves are poorly characterized. MCM-41 materials belong to the family of mesoporous silicas exhibiting a hexagonal arrangement of pores with diameters from 15 to 100 Å.[4,5] Large pore sizes of MCM-41 permit reactions involving bulky molecules that are not capable of entering the channels of microporous zeolites. Incorporating metal ions into siliceous MCM-41 enhances electron-transfer efficiency between embedded molecules and the MCM-41 framework.[6−8]

In this work we report oxidation of carotenoids embedded into Fe(III)−MCM-41 molecular sieves. Carotenoids are naturally occurring polyenes with long chains of conjugated double bonds. Carotenoids along with chlorophylls and cytochromes participate in the electron-transfer pathway in photosystem II (PSII).[9,10] They play an essential role as intermediate electron carriers in the reduction of the primary electron donor $P860^+$ by the Cyt b_{559} and Chl_Z.[11−14] The Fe atoms of the cytochromes undergo oxidation and reduction during this process, cycling between the ferrous (Fe^{2+}) and ferric (Fe^{3+}) oxidation states. Examining the electron-transfer reactions of carotenoids within iron-modified MCM-41 molecular sieves is important for understanding the electron-transfer reactions in PSII. Fe(III)-substituted MCM-41 sieves were also used because chemical oxidation of carotenoids by Fe^{3+} ions in organic solvents forms the carotenoid radical cations.[15]

It has been shown that electron paramagnetic resonance (EPR) spectroscopy is a useful technique for characterizing the iron sites in both the low-spin ($S = {}^1/_2$) and high-spin ($S = {}^5/_2$) electronic configurations. Usually in zeolites and molecular sieves the weak field of possible ligands (water, hydroxyl ions, framework oxygen) results in the high-spin ferric ion state that is also characteristic for some iron proteins.[16−18] The spin Hamiltonian for high-spin iron is given by[19,20]

$$H_S = g\beta\mathbf{BS} + D(S_Z^2 - {}^1/_3\mathbf{S}^2) + E(S_X^2 - S_Y^2) + \text{other terms} \quad (1)$$

In this case we can neglect other terms because the symmetry is very close to cubic. The **g** tensor exhibits extremely small anisotropy and the spectral characteristics are determined by the zero field splitting (ZFS) parameters D (axial) and E (rhombic). When the symmetry is axial, $D \neq 0$ and $E = 0$. In the case of rhombic symmetry, $E/D = 1/3$. Most of high spin d^5 systems do not belong to one of the special cases. Several different symmetries at the Fe^{3+} site contribute to multicomponent EPR spectra with overlapping signals. Such complex spectra arising from more than one center can be analyzed at different microwave frequencies. For high-spin Fe^{3+} in proteins and zeolites the electron Zeeman interaction ($g\beta B_0 S$) is much smaller at the X-band frequency than the ZFS interaction.[21,22] This makes interpretation of the EPR spectra difficult due to inhomogeneous broadening arising from the ZFS and overlapping signals. Use of higher microwave frequency is particularly advantageous in this case.

The 9−287 GHz EPR studies were carried out to characterize the Fe^{3+} sites in Fe−MCM-41 molecular sieves. Multifrequency

* To whom correspondence should be addressed. E-mail: lkispert@bama.ua.edu. Fax: (205) 348 9104.

10.1021/jp021565f CCC: $25.00 © 2003 American Chemical Society
Published on Web 12/31/2002

CHART 1

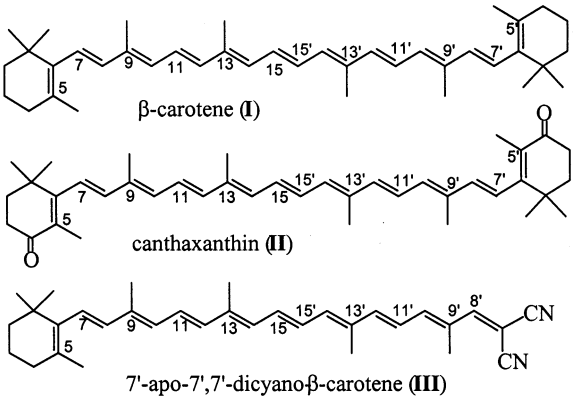

EPR measurements were also performed to elucidate the types of iron sites which are responsible for carotenoid oxidation, their stability and accessibility. Orientation of carotenoid molecules inside Fe−MCM-41 was characterized by electron nuclear double resonance (ENDOR) spectroscopy.

Experimental Section

Synthesis of MCM-41 and Fe−MCM-41. The procedure used for the preparation of the siliceous material (MCM-41) was similar to that reported by Beck et al.[23] First, tetrabutylammonium silicate (TBAS) was prepared in a 10:1 ratio (w/w) from tetrabutylammonium hydroxide (40 wt %, Aldrich) and fumed silica (Sigma). Then 20.3 g of cetyltrimethylammonium chloride (CTAC, 25 wt %, Aldrich) and 12.21 g of TBAS were mixed with 5.94 g of H_2O. Finally, 5.91 g of fumed silica was dissolved in the mixture. The resulting gel was placed in a Teflon bottle and heated for 6 days at 95 °C, cooled to room temperature, washed with deionized water, and finally dried in air. The template CTAC was removed by calcination in air at 530 °C for 18 h. The resulting white powder is called MCM-41.

Fe−MCM-41 was synthesized by ion-exchange according to the literature.[24] A 0.8 g aliquot of MCM-41 and 30 mL of 0.1 M $FeCl_3 \cdot 6H_2O$ ethanol solution were mixed. The mixture was stirred for 3 h at 60 °C. After reaction, the solid was washed with water to remove any ions adsorbed on the external surface. Then it was dried at room temperature and placed in an oven at 100 °C for 24 h. The sample was then calcined at 450 °C in air for 2 h for. A white solid was produced with an iron content of 1.6%. The white solid was designated as Fe−MCM-41.

Sample Preparation. β-Carotene was supplied by Sigma and canthaxanthin by Fluka. The synthesis and characterization of 7′-apo-7′,7′-dicyano-β-carotene has been described previously.[25] Carotenoid structures are shown in Chart 1. The purity of the carotenoids was checked by ^{1}H NMR (360 MHz, $CDCl_3$) and TLC analyses. The carotenoids were stored at −14 °C in a desiccator containing drierite. The solvent, methylene chloride, CH_2Cl_2 (Aldrich, anhydrous), was stored under nitrogen in a drybox and used without further purification.

Fe−MCM-41 samples were activated by heating at 260−360 °C for 5−12 h in air in a quartz EPR tube before use to remove water molecules and OH ions adsorbed on the surface, cooled to room temperature, and then the carotenoid solution was added to the sample. Carotenoid solutions in CH_2Cl_2 (10^{-2} to 10^{-3} M) were degassed before use by three freeze−pump−thaw cycles. The solvent was evaporated under reduced pressure, and the tube was evacuated and sealed. The samples were stored at 77 K. Irradiation of the Car/MCM-41 samples was carried out at 350 nm (77 K) with a Xe/Hg lamp (1 kW) equipped with a Kratos monochromator.

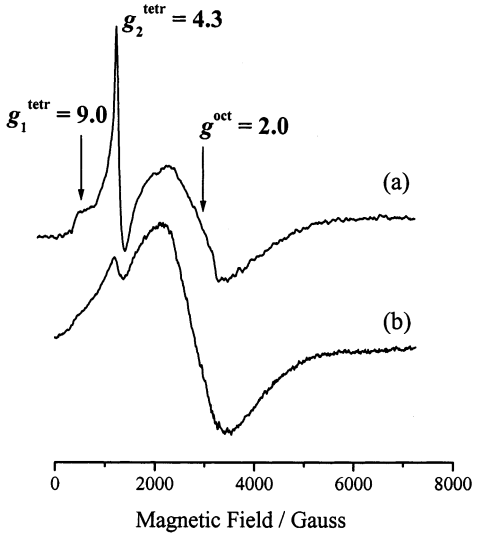

Figure 1. X-band EPR spectra of Fe(III)−MCM-41 activated at (a) 260 °C and (b) 360 °C and measured at 77 K.

EPR Measurements. X-band (9 GHz) EPR and ENDOR measurements were carried out with a Bruker ESP 300E EPR spectrometer, containing a DICE ENDOR ESP 350 system and a temperature controller. The magnetic field was measured with a Bruker EPR 023M gaussmeter, and the microwave frequency was measured with a model HP 5352B microwave frequency counter.

The 95−287 GHz measurements were performed at the high-field EPR facility of the National High Magnetic Field Laboratory (Tallahassee, FL). The spectrometer used was analogous to that described by Mueller et al.[26] The fundamental microwave frequencies of 95 ± 3 and 110 ± 3 were generated by two Gunn oscillators, whereas higher harmonics of these were produced with a frequency multiplier. An EIP 578 frequency counter measured and locked the fundamental frequency. The 15 T Oxford Instruments superconducting magnet was typically swept at a rate in the range of 0.5 to 6 mT/s. A modulation coil around the sample space produced 1−5 mT of field modulation at 8 kHz. As the spectrometer operated in a single-pass transmission mode without resonator, a similarly sized sample could be measured at all frequencies. The samples were contained in a sealed 4 mm quartz EPR tube and placed in an Oxford Instruments CF 1200 continuous flow cryostat. A liquid helium cooled hot-electron InSb bolometer (QMC Instruments, U.K.) served as the (sub)millimeter-wave detector.

The XSophe computer simulation program was used for spectral simulation.

Results and Discussion

Multifrequency Study of the Fe−MCM-41 Molecular Sieves. The X-band EPR spectrum of Fe−MCM-41 activated at 260 °C and recorded at 77 K consists of a strong sharp peak at $g = 4.3$ with a shoulder at $g = 9.0$ (Figure 1a). The presence of these signals originating from the middle Kramers doublet and the lowest Kramers doublet, respectively, is characteristic of high-spin Fe^{3+} when $E/D = 1/3$.[27,28] The observation of a $g = 4.3$ signal in zeolites and aluminophosphate molecular sieves is usually considered as evidence for the presence of framework Fe^{3+} ions.[29−32] The framework iron species are tetrahedrally coordinated with four oxygen atoms in the first shell and four Si atoms in the second shell. The tetrahedron shows strong

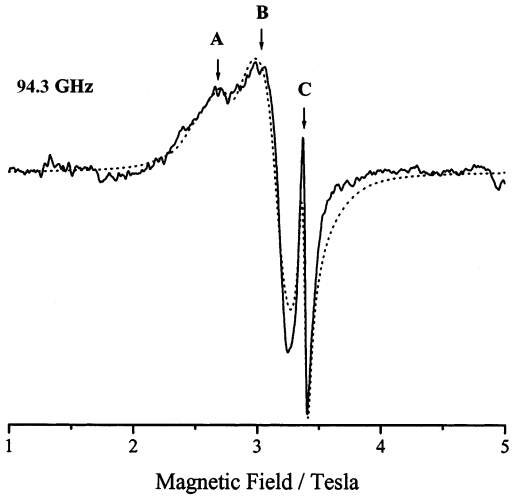

Figure 2. EPR spectra of Fe(III)−MCM (solid line) measured at 94.3 GHz, modulation 2.36 kHz, 180 mA, 5 K; (dotted line) simulated.

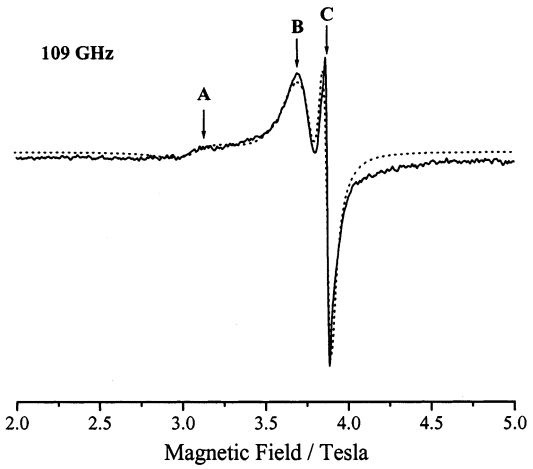

Figure 3. EPR spectra of Fe(III)−MCM (solid line) measured at 109 GHz, modulation 6.5 kHz, 5 K; (dotted line) simulated.

rhombic distortion because two Fe−O bond distances for which oxygen atoms are involved in hydrogen bonds are longer than two others. The X-band spectrum of Fe−MCM-41 also exhibits a broad (∼2000 G) signal with $g \approx 2$. A $g = 2.0$ signal in zeolites is commonly assigned to extraframework Fe^{3+} ions.[29−32] However, if the $g = 4.3$ and $g = 9.0$ signals are from the lower and middle Kramers doublets, we should also expect a contribution from the framework Fe originating from the upper Kramers doublet to the $g = 2$ signal. Figure 1b shows that activation of Fe−MCM-41 at higher temperature (Figure 1b) diminishes the $g = 4.3$ framework iron signal and significantly increases the extraframework iron signal at $g = 2.0$. This is consistent with observation that tetrahedral coordination of the framework Fe^{3+} ions is not very stable.[32] It has been shown that thermal treatment leads to dislocation of Fe^{3+} ions from the silica walls and enlargement of extraframework iron species, probably in the form of dispersed oxide particles.[31]

To obtain additional information regarding the different types of Fe^{3+} sites in Fe−MCM-41 EPR measurements at higher microwave frequencies were carried out. It was found that the $g = 4.3$ signal is not observed at the 94.3 GHz and higher frequencies (Figures 2−5). It has been reported for iron-containing zeolites that the $g = 4.3$ signal disappeared even at Q-band (35 GHz).[29] We suppose that the $g = 4.3$ and $g = 9.0$ signals correspond not to the $M_S = \pm 1/2$, but to the $M_S = \pm 3/2$ and $M_S = \pm 5/2$ transitions. At low field (X-band) these

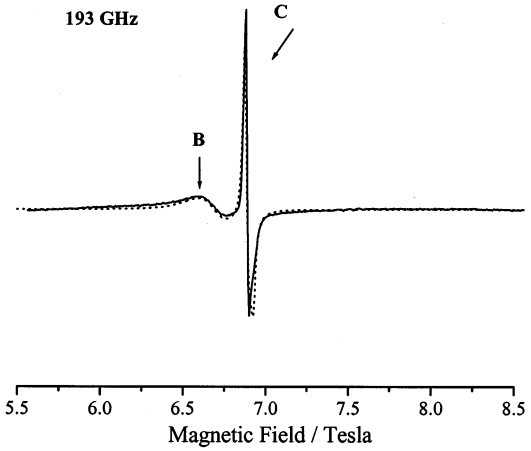

Figure 4. EPR spectra of Fe(III)−MCM (solid line) measured at 193 GHz, modulation 6.5 kHz, 5 K; (dotted line) simulated.

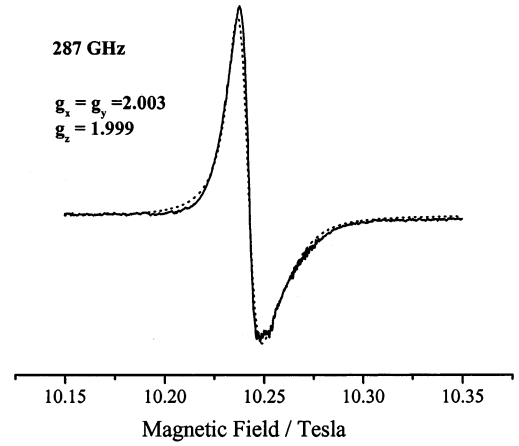

Figure 5. EPR spectra of Fe(III)−MCM (solid line) measured at 287 GHz, modulation 6.5 kHz, 5 K; (dotted line) simulated.

transitions have appreciable intensity as the higher order terms (the second and fourth order ZFS) mix the states. At high field the Zeeman interaction is dominating and the transitions are more forbidden.

In contrast, the shape of the $g = 2.0$ signal is better determined at higher frequencies. At 94.3 GHz (Figure 2) the $g = 2.0$ line is resolved into two broad peaks (A and B) and an intense narrow signal (C). To determine g values and the ZFS parameters D and E for different Fe^{3+} signals spectral simulations were performed using the XSophe program based on eq 1. The program includes a powder matrix diagonalization approach that is important for high spin iron systems.[33,34] Simulations were carried out using a Gaussian line shape and varied isotropic line width, E/D ratio, and g values. The parameters obtained at higher frequencies were used for spectral simulations at lower frequencies. Simulated parameters are given in Table 1.

The $g = 2.45$ and $g = 2.07$ signals observed at 94.3 GHz (Figure 2) and at 109 GHz (Figure 3) could be the **g** tensor components of the same iron center. However, they have different ZFS parameters. Therefore, we attributed these signals to different iron sites. The peaks at $g = 2.3-2.5$ are commonly assigned to aggregated iron species that can possess ferromagnetic properties.[29−32] It has been shown by means of electron spin−echo (ESE) experiments[29] that Fe^{3+} species with such g values do not contribute to the echo because of a strong spin−spin interaction. The formation of such iron clusters with $g = 2.45$ ($E/D = 0.033$) most likely is a result of high-temperature extraction of framework Fe^{3+} followed by the formation of ferric

TABLE 1: Simulated EPR Parameters of High-Spin Fe^{3+} Sites in Fe−MCM-41

iron sites	*g*-values	*E*/*D*	*D*/cm^{-1}
	I. Framework Iron		
(a) Fe^{3+} in tetrahedral coordination	$g = 4.3$	0.33	0.3 ± 0.1
(b) single Fe^{3+} site	$g_x = g_y = 2.003$ $g_z = 1.99$	0.3	0.013 ± 0.005
	II. Extraframework Iron		
(a) iron clusters	$g = 2.45$	0.033	0.6 ± 0.1
(b) Fe^{3+} on the surface of the pore	$g = 2.07$	0.02	0.42 ± 0.15

oxide particles when Fe^{3+} is incorporated at a high content (1.6%) in MCM-41. The $g = 2.07$ ($E/D = 0.02$) signal can be due to the extraframework iron in interstitial oxide (hydroxide) phases. Abstraction of a water molecule from ferric hydroxide and nearby terminal Si−OH can form an isolated Fe^{3+} coordinated to the surface oxygen and located on the surface of the mesopore as an Fe−O−Si site.[31,32]

It should be noted that the line width of the signals decreases with increasing frequency from 94.3 to 287 GHz. If the broadening mechanism is limited to the ZFS only, a narrowing should be expressed by the ratio of the spectrometer frequencies.[29] However, in this case the Fe^{3+} narrowing is different from the expected value. This indicates the existence of other sources of broadening such as overlapping signals of different species, spin−spin interaction and so on. For instance, the line width of the narrow signal C changes from 49 mT at 109 GHz to 38 mT at 193 GHz and to 20 mT at 287 GHz. This narrowing indicates that the signal is most likely due to Fe^{3+} ions. The 287 GHz spectrum of Fe−MCM-41 exhibits only one slightly asymmetric single line (Figure 5). Spectral simulation gives the best fit with $g_x = g_y = 2.003$, $g_z = 1.99$, and $E/D = 0.3$. Observation of a unique narrow line with $g \sim 2$ at the X and Q bands has been reported for ferrisilicate with low iron loading and attributed to a single Fe^{3+} site with a *D* value in the range of a few hundred gauss.[29] We suggest that this narrow signal with considerable rhombic distortion $E/D = 0.3$ ($D = 0.013$ cm^{-1}) is due to a single framework "defect like" iron site. This is consistent with the assertion that framework Fe^{3+} can contribute to the $g = 2$ signal.[29]

Incorporation of Carotenoids. The approximate Fe−MCM-41 pore size (35 Å) was estimated by X-ray powder diffraction measurements, as has been reported earlier.[8] The pore size of 35 Å is large enough to accommodate carotenoids with average length 25−30 Å inside the pore. β-Carotene (I), canthaxanthin (II), and 7′-apo-7′,7′-dicyano-β-carotene (III) were incorporated into Fe−MCM-41. Figure 6 compares X-band EPR spectra of Fe−MCM-41 before (a) and after (b, c) carotenoid III adsorption. The sample with incorporated III exhibits a signal with $g = 2.0028 \pm 0.0002$, characteristic of the carotenoid radical cation prior to irradiation (Figure 6b). Irradiation of the samples at 365 nm (77 K) increases the $Car^{\bullet+}$ signal intensity (Figure 6c). The X-band experiments (Figure 6) showed that adsorption of the carotenoid results in a decrease of the broad $g = 2.0$ signal whereas the intensity of the Fe^{3+} signal at $g = 4.3$ does not change significantly. Adsorption of carotenoids I and II also leads to a decrease of the $g = 2.0$ signal intensity. However, in this case the $Car^{\bullet+}$ signals were not observed before irradiation. The X-band measurements cannot identify which one of the iron sites can react with carotenoid. Only the 94 GHz measurements (Figure 7) were able to demonstrate that adsorption of carotenoid results in a significant decrease of the $g = 2.07$ signal whereas the intensities of the $g = 2.45$ signal and the narrow line with $g_x = g_y = 2.003$, $g_z = 1.999$ are almost not affected. The results show that the extraframework Fe^{3+} ions located on the surface of the pore are primarily responsible for carotenoid oxidation. Probably, these sites are more accessible for bulky organic molecules than the framework iron within silica walls.

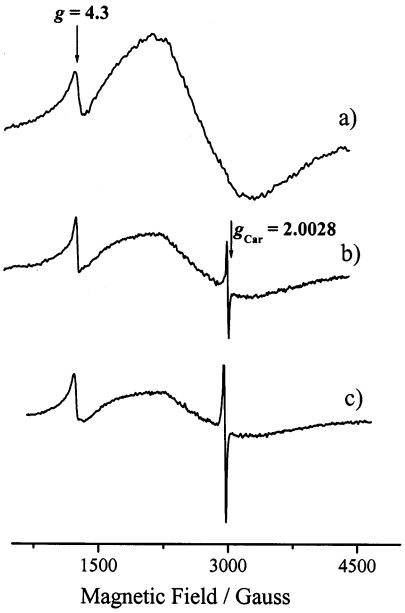

Figure 6. X-band EPR spectra of Fe(III)−MCM-41 (a) activated at 360 °C and measured at 77 K; (b) after adsorption of 7′-apo-7′,7′-dicyano-β-carotene (77 K); (c) after irradiation at 365 nm for 2 min.

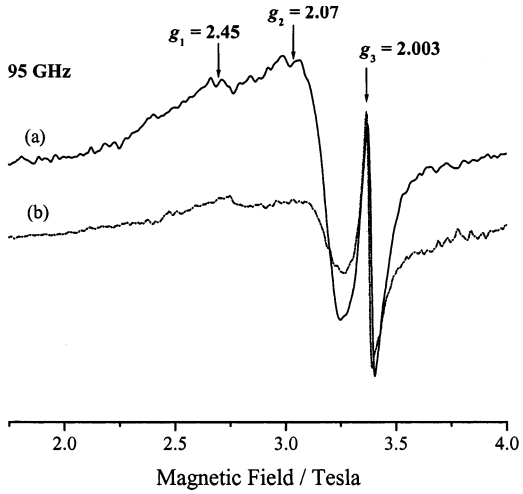

Figure 7. 95 GHz EPR spectra of Fe−MCM-41 (a) in the absence of carotenoid; (b) after adsorption of canthaxanthin.

When carotenoid incorporated in Fe−MCM-41 was subjected to irradiation at 365 nm for 2 min, other paramagnetic species besides the $Car^{\bullet+}$ were detected. No such radicals were observed in the absence of carotenoids prior to or after irradiation. Figure 8 shows the 9.1 GHz (insert) and 108 GHz EPR spectra of canthaxanthin irradiated in Fe−MCM-41 and measured at 77 and 5 K, respectively. Spectral simulation allows determination of the carotenoid radical cation ($g = 2.0026$) and a signal arising from species with $g_1 = 2.015$, $g_2 = 2.006$, and $g_3 = 2.00$. Signals with similar parameters have been observed in γ-irradiated siliceous Al− and Ti−MCM-41 and attributed to Si−O$^{\bullet}$−Si or Al−(Ti)−O$^{\bullet}$−Si units of the framework, so-called V centers.[35] It has been shown that the V centers in Ti−MCM-41[35] are formed during the reduction of Ti^{4+} to Ti^{3+} (the EPR signal of Ti^{3+} was detected) followed by electron stabilization on the oxygen atom. Oxygen radicals have also been detected in Ni(II)−MCM-41 after adsorption of CO or D_2O molecules and assigned to Ni(I)−$O_2^{\bullet-}$ species.[36−38] We suppose that

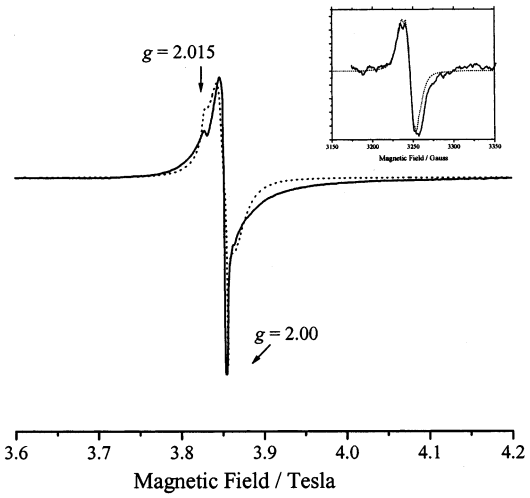

Figure 8. 108 GHz EPR spectrum of irradiated at 77 K canthaxanthin in Fe(III) MCM-41 and measured at 5 K, (insert) X-band EPR spectrum of irradiated canthaxanthinin Fe(III)−MCM-41 measured at 77 K.

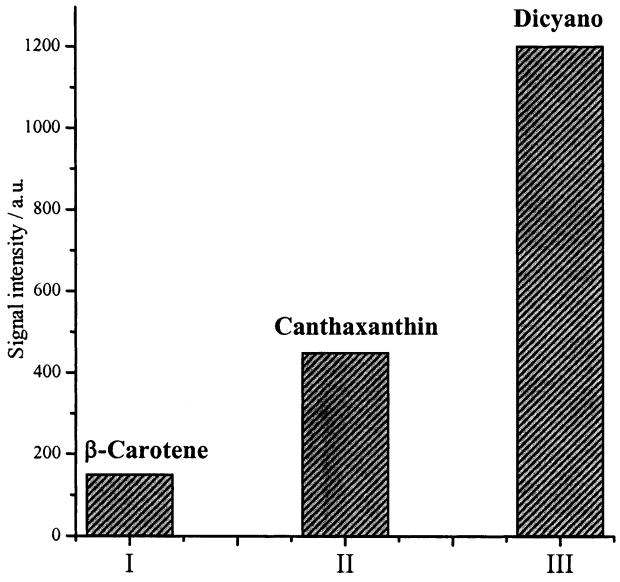

Figure 9. Yield of I−III carotenoid radical cations in Fe−MCM-41 molecular sieves.

oxidation of carotenoids in Fe−MCM-41 proceeds through electron transfer from carotenoid molecules to the electron acceptor sites (Fe^{3+} coordinated with surface oxygen atoms) producing $Fe^{2+}-O^{\bullet}-Si$ species:

$$Car + Fe^{3+}-O-Si \rightarrow Car^{\bullet+} + Fe^{2+}-O^{\bullet}-Si$$

Figure 9 shows that the $Car^{\bullet+}$ yield (the $Car^{\bullet+}$ EPR signal intensity) in Fe−MCM-41 increases in the order β-carotene < canthaxanthin < dicyano. It should be noted that the first oxidation potentials of the carotenoids are 0.54, 0.69, and 0.74 V for β-carotene, canthaxanthin, and dicyano, respectively.[39] The fact that formation of $Car^{\bullet+}$ decreases in yield with decreasing oxidation potential is surprising. On the other hand, the yield depends not only on the ease of formation but also on the stability of the generated radicals. For instance, β-carotene (I) in polar solvents exhibits an inversion of its first and second oxidation potentials.[40] This facilitates the formation of a diamagnetic dication of I (I^{2+}) and, hence, explains the low yield of $I^{\bullet+}$. The presence of different terminal groups in Car can also provide stabilization of $Car^{\bullet+}$ on the solid support as a result of specific interactions of the carotenoid with a matrix. Our

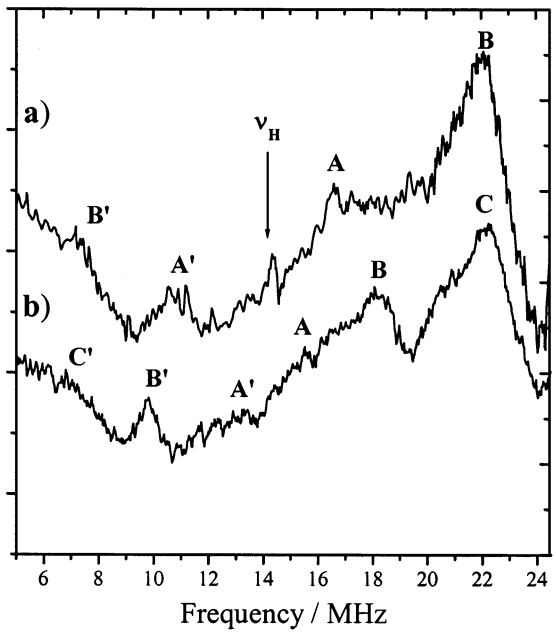

Figure 10. ENDOR spectra of (a) 7′-apo-7′,7′-dicyano-β-carotene; (b) canthaxanthin in Fe−MCM-41 irradiated at 77 K and measured at 120 K at MW frequency of 9.5 GHz, MW power of 20.2 mW, modulation frequency of 12.5 kHz, RF power of 150 W conversion time 40 s, 20 scans.

previous results demonstrated that Car with a terminal carboxy group when adsorbed on TiO_2 forms long-lived radical cations because of covalent bonding of the carotenoid to the surface.[41] Carotenoid III (7′-apo-7′,7′-dicyano-β-carotene) gives the largest yield of $Car^{\bullet+}$ in Fe(III)−MCM-41 that may be due to the interaction between Fe^{3+} and the nitrogen atoms of the two cyano groups. Iron is a well-known chelating agent in biology and oxidative catalysis. Oxidation of amines coordinated to iron ions has been reported.[42,43] Series of iron−cyano complexes have been prepared and characterized.[44,45] A mechanism of cyano-compound oxidation has been proposed in which the Fe^{3+}−cyano complex is involved as an intermediate.[46] We propose that strong interaction between the cyano-groups in III and Fe^{3+} ions may facilitate stability of the $III^{\bullet+}$ in Fe−MCM-41.

Comparative ENDOR measurements for carotenoid III and canthaxanthin in Fe−MCM-41 were carried out. Figure 10 shows the ENDOR spectra of Fe−MCM-41 with incorporated carotenoid III (Figure 10a) and canthaxanthin (Figure 10b) irradiated at 77 K and recorded at 120 K. The ^1H powder ENDOR spectrum of III exhibits two groups of signals (A and B) placed symmetrically around the free proton frequency 14.5 MHz with hyperfine coupling constants of 6.8 and 12.6 MHz. These hyperfine couplings are most likely due to the protons of freely rotating methyl groups $C(13)C_\beta H_3$ and $C(9)C_\beta H_3$, respectively. Assignment of the coupling constants to specific methyl protons is based on a comparison with previously obtained experimental and simulated parameters for the dicyano radical cation adsorbed on silica gel.[47] Compared to proton signals on silica gel, the $C(9')C_\beta H_3$ and $C(13')C_\beta H_3$ methyl protons are not resolved in the ENDOR spectrum of carotenoid III in Fe−MCM-41. This indicates strong interaction of the terminal cyano groups with the surface, resulting in restricted rotation of the $C(9')C_\beta H_3$ and $C(13')C_\beta H_3$ methyl groups and significant line broadening. This provides indirect evidence for the coordination of the carotenoid through the cyano groups to iron ions located on the surface of the pore. The proton ENDOR spectrum of canthaxanthin (Figure 10b) contains three groups

of signals (A, B, and C). On the basis of our previous results obtained for canthaxanthin on silica−alumina surface[48] the determined hyperfine couplings 2.2, 8.6, and 13.8 MHz may be assigned to the C(5,5′)$C_\beta H_3$, C(9,9′)$C_\beta H_3$, and C(13,13′)-$C_\beta H_3$ methyl protons, respectively. ENDOR data demonstrate that all methyl protons of canthaxanthin are well-resolved in Fe−MCM-41 compared to those obtained on silica alumina,[48] where the lines of the central C(13,13′)$C_\beta H_3$ methyl protons are broadened because of restricted motion. The results indicate a different orientation of the carotenoids II and III within Fe−MCM-41. Although carotenoid III is strongly coordinated to the surface of the pore via the terminal cyano groups, carotenoid II is bound via both ends of the polyene chain providing free rotation of the methyl groups.

Conclusions

Here we report 9−287 GHz EPR measurements of Fe(III)−MCM-41 mesoporous molecular sieves with incorporated carotenoids. The X-band spectrum exhibits a sharp signal at $g = 4.3$ with a shoulder at $g = 9.0$, which is characteristic of high-spin Fe(III) in the case when $E/D = 1/3$. Disappearance of these signals at 94 GHz and higher frequencies is probably related to the fact that (1) the eigenstates are close to pure $M_S = \pm 1/2$, $\pm 3/2$, and $\pm 5/2$ states and the transitions observed at low fields are forbidden; (2) the transitions will broaden in this nonoriented sample.

Measurements at 94 GHz and higher frequencies showed that the $g = 2.0$ region consists of overlapping signals from Fe^{3+} sites with different ZFS. The peak with $g = 2.45$ is tentatively assigned to aggregated Fe^{3+}. Additional pulsed EPR experiments are necessary to detect strong spin−spin interactions and identify the nature of these species. The signal with $g = 2.07$ can be attributed to Fe^{3+} coordinated to oxygen atoms on the surface of the pore. A unique narrow line with $g_x = g_y = 2.003$, $g_z = 1.99$, and $E/D = 0.3$ was attributed to a single framework Fe^{3+} site.

Incorporation of carotenoids into Fe−MCM-41 results in carotenoid radical cation generation. The 9−94 GHz EPR measurements demonstrated that extraframework iron species at the surface of the pore (the $g = 2.07$ signal) are mostly responsible for carotenoid oxidation in molecular sieves because of their accessibility for interaction with large organic molecules. An increase of the concentration of such sites improves the catalytic and adsorption properties of Fe−MCM-41 considerably. The yield of $Car^{\bullet+}$ formation decreases in the order 7′-apo-7′,7′-dicyano-β-carotene > canthaxanthin > β-carotene. The largest yield of $III^{\bullet+}$ in Fe(III)−MCM-41 is probably due to complexation between Fe^{3+} ions and the cyano groups of the carotenoid. ENDOR measurements confirmed strong interaction of III with the pore surface through the dicyano end.

Acknowledgment. This work was supported by the Division of Chemical Sciences, Office of Basic Energy Sciences, Office of Energy Research, the U.S. Department of Energy, Grant DE-FG02-86ER13465 and the NSF supported National High Magnetic Field Laboratory (Tallahassee, FL).

References and Notes

(1) Feng, X.; Hall, W. K. *J. Catal*. **1997**, *168*, 368.
(2) Chen, H.-Y.; Sachtler, W. M. H. *Catal. Today* **1998**, *42*, 73.
(3) Volodin A. M.; Dubkov, K. A.; Lund, A. *Chem. Phys. Lett*. **2001**, *333*, 41.
(4) Beck, J. S.; Vatuli, J. C.; Roth, W. J.; Lewnowitz, M. E.; Kresge, C. T.; Schmit, K. D.; Chu, C. T.-W.; Olson, D. H.; Sheppard, E. W.; McCullen, S. B.; Higgins, J. B.; Schlenker, J. L. *J. Am. Chem. Soc.* **1992**, *114*, 10834.
(5) Anwander, R.; Nagl, I.; Widenmeyer, M.; Engelhardt, G.; Groeger, O.; Palm, C.; Röser, T. *J. Phys. Chem. B* **2000**, *104*, 3532.
(6) Hartmann, M.; Püppl, A.; Kevan, L. *J. Phys. Chem*. **1996**, *100*, 9906.
(7) Hyung-Suh, H. M.; Luan, Z.; Kevan, L. *J. Phys. Chem. B* **1997**, *101*, 10455.
(8) Konovalova, T. A.; Gao, Y.; Schad, R.; Kispert, L. D.; Saylor, C. A.; Brunel, L.-C. *J. Phys. Chem. B* **2001**, *105*, 7459.
(9) Truscott, T. G. J. *Photochem. Photobiol. B Biol*. **1990**, *6*, 359.
(10) Mathis, P.; Rutherford, A. W. *Biochim. Biophys. Acta* **1987**, *767*, 217.
(11) Zoumi, A.; Witt, H.-T.; Kern, J.; Fromme, P.; Krauss, N.; Saenger, W.; Orth, P. *Nature* **2001**, *409*, 739.
(12) Thompson, L. K.; Brudvig, G. W. *Biochemistry* **1988**, *27*, 6653.
(13) Hillman, B.; Schlodder, E. *Biochim. Biophys. Acta* **1997**, *1231*, 76.
(14) Faller, P.; Pascal, A.; Rutherford, A. W. *Biochemistry* **2001**, *40*, 6431.
(15) Jeevarajan, J. A.; Wei, C. C.; Jeevarajan, A. S.; Kispert, L. D. *J. Phys. Chem*. **1996**, *100*, 5637.
(16) Smith, T. D.; Pilbrow, J. R. In *ESR of Iron Proteins*; Berliner, L. J., Reuben, J., Eds.; Biological Magnetic resonance, Vol. 2; Plenum Press: New York, 1980; p 85.
(17) Boussac, A.; Sugiura, M.; Inoue, Y.; Rutherford, A. W. *Biochemistry* **2000**, *39*, 13788.
(18) Hans, M.; Buckel, W.; Bill, E. *Eur. J. Biochem*. **2000**, *267*, 7082.
(19) Dowsing, R. D.; Gibson, J. F. *J. Chem. Phys*. **1969**, *50*, 294.
(20) Sweeney, W. V.; Coucouvanis, D.; Coffman, R. E. *J. Chem. Phys*. **1973**, *59*, 369.
(21) Wickman, H. H.; Klein, M. P.; Shirly, D. A. *J. Phys. Chem*. **1965**, *42*, 2113.
(22) Oosterhuis, W. T. *Struct. Bonding* **1974**, *20*, 19.
(23) Beck, J. S.; Vartuli, J. C.; Roth, W. J.; Leonowicz, M. E.; Kresge, C. T.; Schmit, K. D.; Chu, T.-W.; Olson, D. H.; Shepperd, E. W.; McCullen, S. B.; Higgins, J. B.; Schlenker, J. L. *J. Am. Chem. Soc.* **1992**, *114*, 10834.
(24) Bourlinos, A. B.; Karakassides, M. A.; Petridis, D. *J. Phys. Chem. B* **2000**, *104*, 4375.
(25) Hand, E. S.; Belmore, K. A.; Kispert, L. D. *Helv. Chim. Acta* **1993**, *76*, 1939.
(26) Mueller, F.; Hopkins, M. A.; Coron, N.; Grynberg, M.; Brunel, L. C.; Martinez, G. *Rev. Sci. Instrum.* **1989**, *60*, 3681.
(27) Pilbrow, J. R. *Transition Ion Electron Paramagnetic Resonance*; Clarendon Press: Oxford, U.K., 1990; pp 125−144.
(28) Abragam, A.; Bleany, B. In *Electron Paramagnetic Resonance of Transition Metal Ions*; Clarendon Press: Oxford, U.K., 1970; pp 156−163.
(29) Goldfarb, D.; Bernardo, M.; Strohmaier, K. G.; Vaughan, D. E. W.; Thomann, H. *J. Am. Chem. Soc*. **1994**, *116*, 6344.
(30) Yuan, Z. Y.; Liu, S. Q.; Chen, T. H.; Wang, J. Z.; Li, H. X. *Chem. Soc. Chem. Commun.* **1995**, 973.
(31) Tuel, A.; Acron, I.; Miller, J. M. M. *J. Chem. Soc., Faraday Trans*. **1998**, *94*, 3501.
(32) Kosslick, H.; Lischke, G.; Landmesser, H.; Parlitz, B.; Storek, W.; Fricke, R. *J. Catal*. **1998**, *176*, 102.
(33) Yang, A.-S.; Gaffney, B. J. *Biophys. J.* **1987**, *51*, 55.
(34) Gaffney, B. J.; Mavrophilipos, D. V.; Doctor, K. S. *Biophys. J.* **1993**, *64*, 773.
(35) Prakash, A. M.; Sung-Suh, H. M.; Kevan, L. *J. Phys. Chem. B* **1998**, *102*, 857.
(36) Prakash, A. M.; Kevan, L. *J. Phys. Chem*. **1996**, *100*, 19587.
(37) Hartmann, M.; Püppl, A.; Kevan, L. *J. Phys. Chem*. **1996**, *100*, 9906.
(38) Chang, Z.; Zhu, Z.; Kevan, L. *J. Phys. Chem*. **1999**, *103*, 9442.
(39) Liu, D.; Kispert, L. D. *Electrochemical aspects of carotenoids*. In *Recent Research Developments in Electrochemistry*; Pandalai, S. G., Ed.; Transworld Research Network: Trivandrum, India, 1999; pp 139−157.
(40) Hapiot, P.; Kispert, L. D.; Konovalov, V. V.; Saveant, J.-M. *J. Am. Chem. Soc*. **2001**, *123*, 6669.
(41) Konovalova, T. A.; Kispert, L. D.; Konovalov, V. V. *J. Phys. Chem. B* **1999**, *103*, 4672.
(42) Goto, M.; Kanda, N.; Sakai, T.; Goedken, V. *Inorg. Chem*. **1985**, *24*, 582.
(43) Goedken, V. *J. Chem. Soc., Chem. Commun*. **1972**, 207.
(44) Barefield, E. K.; Mocella, M. T. *J. Am. Chem. Soc*. **1975**, *97*, 4238.
(45) Ridd, M. J.; Keene, F. R. *J. Am. Chem. Soc*. **1981**, *103*, 5733.
(46) Casta Ferreira, A. M.; Toma, H. E. *J. Chem. Soc., Dalton Trans*. **1983**, 2051.
(47) Piekara-Sady, L.; Jeevarajan, A. S.; Kispert, L. D. *J. Chem. Soc., Faraday Trans*. **1995**, *91*, 2881.
(48) Jeevarajan, A. S.; Kispert, L. D.; Piekara-Sady, L. *Chem. Phys. Lett*. **1993**, *209*, 269.